J. Wind Eng. Ind. Aerodyn. 99 (2011) 1000–1010

Contents lists available at ScienceDirect

Journal of Wind Engineering and Industrial Aerodynamics

journal homepage: www.elsevier.com/locate/jweia

# Wind tunnel tests on heavy road vehicles: Cross wind induced loads—Part 1

F. Cheli, R. Corradi, E. Sabbioni, G. Tomasini *

*Department of Mechanical Engineering, Politecnico di Milano, Via La Masa 1, 20156 Milano, Italy*

ARTICLE INFO

Available online 24 August 2011

*Keywords:*
Wind tunnel tests
Road heavy vehicles
Cross wind
Aerodynamic force and moment coefficients
Aerodynamic pressure coefficients
Vehicle admittance function

ABSTRACT

In the recent years, rollover has become an important safety issue for a large class of vehicles. Even though rollovers constitute a small percentage of all accidents, they have unproportionally large contribution to severe and fatal injuries. Under this point of view, rollover of heavy vehicles is particularly critical being associated with large traffic disruption, economic loss and risks connected to the transported goods. One of the main causes for heavy vehicles rollover is recognised to be cross wind. In order to determine which parameters (geometry and vehicle type, infrastructure scenario, turbulence conditions, etc.) most affect the aerodynamic loads acting on heavy vehicles, a comprehensive experimental campaign has been carried out in the Politecnico di Milano wind tunnel. The overall activity is presented in 2 papers. In this first paper attention is focused on a high-sided lorry in flat ground scenario. Mean aerodynamic forces and moments have been measured by means of a six-components dynamometric balance for different yaw angles and turbulence conditions. Moreover, in order to gain an insight of the flow pattern around the vehicle, pressure distribution on the vehicle surface has been measured. Finally, the vehicle aerodynamic admittance function has been assessed, for high turbulence conditions, to investigate the unsteady force/moment component. The second paper deals with the effect of infrastructure scenario (flat ground, embankment, double and single viaduct), of position (vehicle placed upwind or downwind) and of vehicle geometry/type (high-sided lorry with and without a trailed unit, tractor-semitrailer combination and tank truck) on the aerodynamic forces and moments, including both steady and unsteady components.



## 1. Introduction

Due to the serious consequences on road/rail transportation safety, the interest towards wind induced rollover of road and rail vehicles has arised during these last years. In fact, trains, high-sided lorries, trucks and tank trucks are particularly at risk of rollover when running on exposed sites such as embankments, viaducts or long span bridges (Baker and Reynolds, 1992; Coleman and Baker, 1992; Baker, 1994; Bocciolone et al., 2008).

Several studies (Cooper, 1984; Baker, 1991a, 1991b; Coleman and Baker, 1994) and EC projects have addressed cross wind induced rollover of road/rail vehicles over the years.

As far as rail vehicles are concerned, a specific task of the BRITE-EURAM TRANSAERO project (1994–1998) was devoted to the study of cross wind effects on rail vehicles (TRANSAERO Consortium, 2002; Baker, 2002). The same occurred for the RAPIDE project (2001). These studies were carried out within the DeuFrako and the Aerodynamic in Open Air (AOA) projects, where a risk analysis associated to cross wind on trains was performed (DEUFRAKO Consortium, 2004; Gautier et al., 2003; Tielkes and Gautier; 2005).

As far as road vehicles are concerned, during the EC project WEATHER (Delaunay et al., 2006) involving, among the others, Birmingham University, Nottingham University and Politecnico di Milano, an alarm system aimed at warning the driver about rollover risk associated to high cross wind was developed. The alarm system includes meteorological sensors on the infrastructure and a risk assessment software, which evaluates the rollover risk based on a probabilistic approach, taking into account vehicle class and topographic effects. During the alarm system development, different techniques (full scale tests, wind tunnel experiments and CFD numerical calculations) for evaluating the mean aerodynamic forces and moments were compared for a high-sided lorry (Sterling et al., 2010; Quinn et al., 2007) to select the most effective approach for tuning the risk assessment software.

In any case (i.e. both rail and road vehicles), all the approaches proposed to estimate rollover risk are based on the assessment of the vehicle mean aerodynamic coefficients. To this end, a comprehensive experimental campaign including different scale heavy-road vehicles models has been carried out in the wind tunnel of Politecnico di Milano. The results of this campaign have been divided into two parts. In this first paper, the wind tunnel tests carried out on a high-sided lorry (called VAN in the

* Corresponding author. Tel.: +39 02 23998480; fax: +39 02 23998492.
*E-mail addresses:* federico.cheli@polimi.it (F. Cheli), roberto.corradi@polimi.it (R. Corradi), edoardo.sabbioni@polimi.it (E. Sabbioni), gisella.tomasini@polimi.it (G. Tomasini).

0167-6105/$ - see front matter © 2011 Elsevier Ltd. All rights reserved.
doi:10.1016/j.jweia.2011.07.009

following) in flat ground scenario are presented. The second paper is devoted to comparing the high-sided lorry with different vehicle types (tankers, tractor semitrailer combinations and multiple units vehicles) and to evaluate the effect of the infrastructure scenario (flat ground, embankment, single and double viaduct) on the aerodynamic forces and moments acting on the vehicles. Both mean and unsteady aerodynamic forces and moments will be presented. In order to gain an insight of the flow pattern around the vehicles, pressure measurements were performed together with force measurements.

As already mentioned, this first paper focuses on the tests carried out on a VAN, considering flat ground scenario. The experimental set-up will be described and the main results will be presented. In particular, the sensitivity of the mean aerodynamic coefficients to the wind–vehicle relative yaw angle and to the wind turbulence intensity (low, mean and high) will be shown. The mean aerodynamic coefficients, obtained by means of force measurements, will be interpreted on the basis of the measured pressure distribution around the vehicle. Finally, the aerodynamic admittance function of the force/moment components, which are more significant from rollover point of view will be shown. Taking into account the spatial correlation of pressures at any two points on the vehicle surface, the aerodynamic admittance function allows to evaluate the unsteady aerodynamic forces and moments acting on a vehicle subjected to turbulent cross wind and thus simulating the vehicle dynamic response (Cheli et al., 2006).

## 2. Experimental set-up

In the first part of the experimental campaign, a high-sided lorry (VAN, Fig. 1), 8 m long, 2.5 m wide and 3.5 m high (full scale dimensions) was tested: the vehicle is the same, which was considered in the WEATHER project (Sterling et al., 2010). The VAN cabin and the wheels were built in resin (RenShape BM5030) through a CNC machine and then they were assembled on the VAN trailer, made of wood.

All the tests presented in this paper have been performed considering a flat ground scenario, representing the vehicle running on a flat and open terrain. This scenario has been reproduced by positioning the vehicle model directly on the wind tunnel floor, as shown in Fig. 1(a).

### 2.1. Force, speed and pressure measurements

The aim of the wind tunnel tests is to assess the aerodynamic loads acting on a vehicle due to cross wind. It is important to point out that a rigid model was used during the tests: this means that the geometric characteristics of the tested vehicle are reproduced, but not its inertial, stiffness and damping properties. Thus the dynamic interaction between the vehicle and the wind cannot be experimentally evaluated.

The aerodynamic loads acting on the vehicle have been measured through a 6 component dynamometric balance placed under the vehicle model and connected to its wheels. Fig. 2 shows the measurement set-up: the balance is placed under the test chamber floor, so that the connection bars between the wheels and the balance are shielded from the wind.

The wind speed was measured through both Pitot tubes, connected to low pressure micromanometers (Furness FC0510, range 200–2000 Pa, accuracy 0.025% FSD), and a multi-hole pressure probe (Turbulent Flow Instrumentation—series 100 Cobra Probe, accuracy $\pm 0.5$ m/s). The latter instrument allows to measure the 3 wind speed components with high frequency

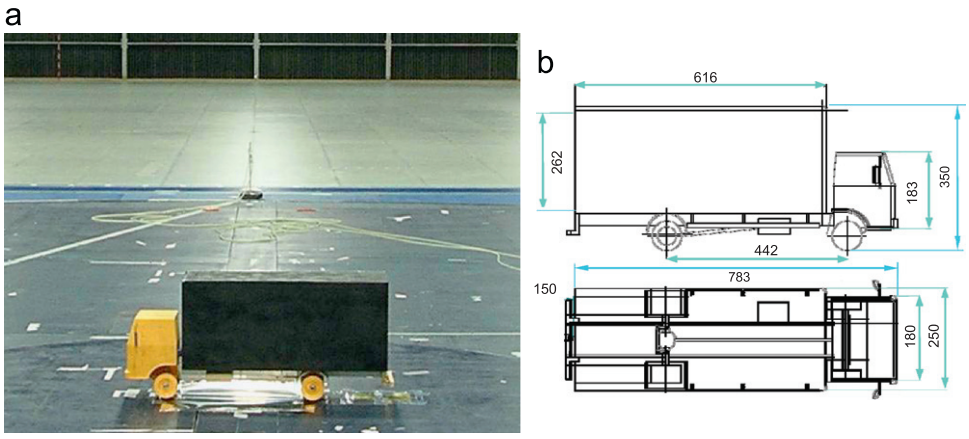


**Fig. 1.** Wind tunnel experimental set-up, VAN vehicle: 1:10 scale model (a) and dimensions (b).

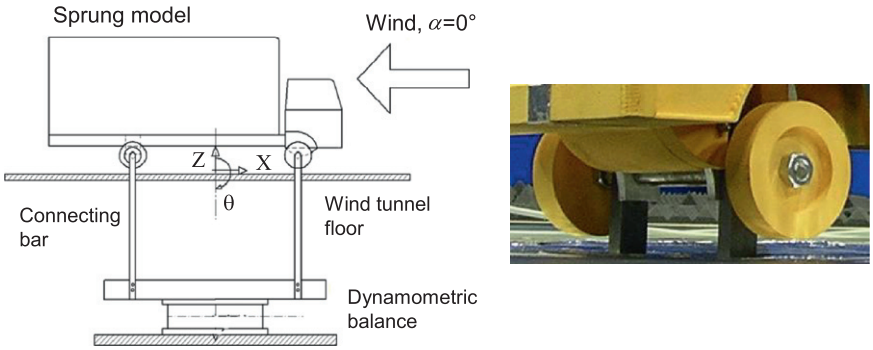


**Fig. 2.** Wind tunnel experimental set-up: connection between the vehicle and the dynamometric balance.

response (up to 20 kHz) within a cone of $\pm 45^{\circ}$. One Pitot tube was placed at a height of 0.6 m (model scale) in order to measure the mean wind speed out of the boundary layer. During the tests with boundary layer simulation, in order to allow the comparison between aerodynamic coefficients assessed in low and mean turbulence conditions, the mean wind speed was also measured through a Pitot tube set in correspondence of the VAN centre of gravity (0.25 m model scale, see Fig. 3). The multi-hole pressure probe was also placed in the latter position during the tests performed to measure the vehicle admittance function.

In addition to the force measurements, in order to investigate the flow pattern around the vehicle, the model was instrumented with 64 pressure taps placed as shown in Fig. 4. The pressure measurements were performed through high-resolution multi-channel pressure scanners (PSI Initium with ESP-DTC scanners), directly set inside the model. All the pressure measurements were synchronous and synchronised with the force measurements.

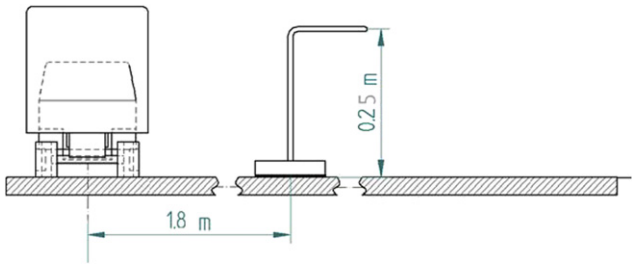


**Fig. 3.** Wind tunnel experimental set-up: anemometer position for flat ground scenario.

### 2.2. Turbulence conditions simulated during wind tunnel tests

In real operation, a vehicle will experience different turbulent wind characteristics, depending on the terrain type where the road is located. In order to evaluate the influence of turbulence on the mean aerodynamic loads acting on the vehicle and to assess the vehicle aerodynamic admittance function, tests were carried out with (mean and high turbulence) and without boundary layer simulation (low turbulence).

The vertical profile of the streamwise velocity $U=U(z)$, normalised with respect to the wind speed $U_{ref}$ measured at the reference height $z_{ref}=0.25$ m (in model scale), is shown in Fig. 5 for three simulated turbulence conditions.

Table 1 summarises the main statistical properties associated with the 3 turbulence conditions reproduced into the wind tunnel, i.e. the turbulence intensity along the wind direction $I_u$ and the

**Table 1**
Wind tunnel experimental set-up: wind characteristics in low, mean and high turbulence conditions measured at the reference height $z_{ref}=0.25$ m (model scale).

| Turbulence | $I_u$ (%) | ${}^{x}L_u$ (m) | ${}^{y}L_u$ (m) |
|---|---|---|---|
| Low | 2 | 0.10 | 0.033 |
| Mean | 20 | 1.185 | 0.3292 |
| High | 26 | 1.72 | 0.68 |

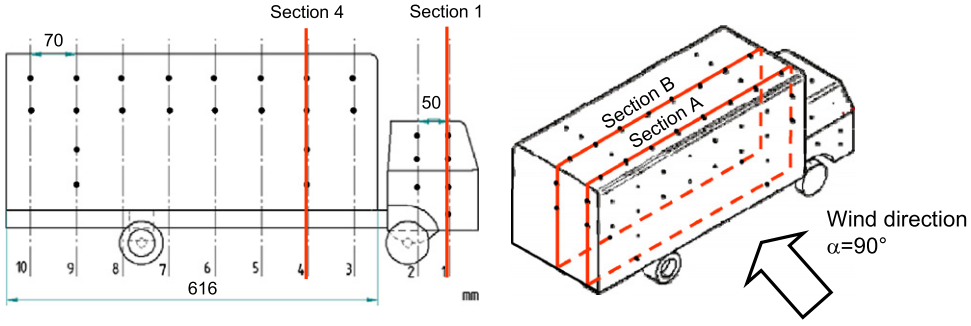


**Fig. 4.** Wind tunnel experimental set-up: pressure taps position on the vehicle.

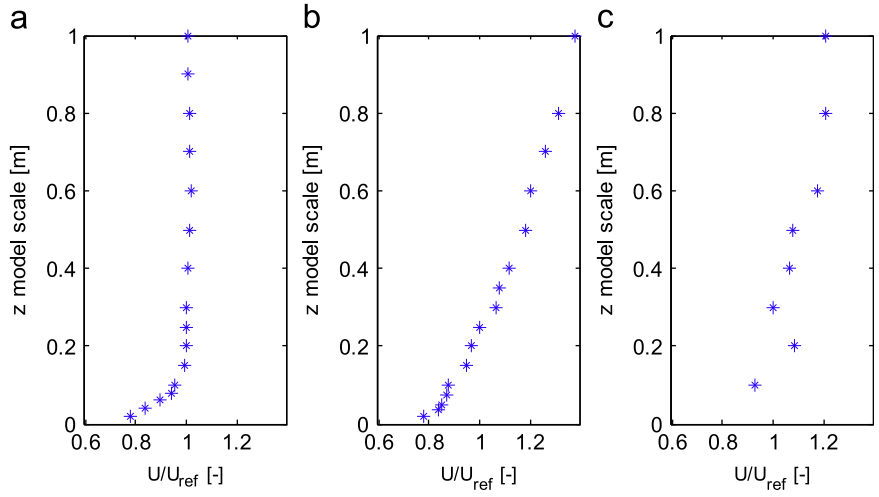


**Fig. 5.** Wind tunnel experimental set-up: normalised streamwise vertical velocity profile ($z_{ref}=0.25$ m, model scale): low turbulence (a), mean turbulence (b) and high turbulence (c).

integral length scales ${}^{x}L_u$ and ${}^{y}L_u$ (ESDU 86010) measured at the reference height $z_{ref}$=0.25 m.

Low turbulence flow results from the standard wind tunnel operating conditions. It is characterised by a uniform vertical profile of the mean wind velocity. In Fig. 5(a), it can be observed that the boundary layer develops for a few centimetres over the floor (15 cm) and, when the gradient is blown over, the mean value of the wind velocity remains constant. This flow condition is characterised by small turbulence intensity and short integral length scales (see Table 1).

During boundary layer simulations, the mean turbulence conditions were generated by positioning in the wind tunnel, before the test section, an array of nine turbulence-producing spires and roughness elements on the chamber floor (Fig. 6). The spires present triangular profile and allow reproducing the velocity gradient, which effectively approximates the atmospheric boundary layer.

For high turbulence conditions, only the array of 9 spires (bigger than those used for the mean turbulence conditions) was adopted. Both in mean (Fig. 5(b)) and in high (Fig. 5(c)) turbulence conditions, the profiles do not reach a constant speed value at the reference height (0.25 m); moreover, due to the roughness elements placed on the floor, the wind speed reduction for lower heights is maximum in medium turbulence conditions.

Mean aerodynamic coefficients and flow pattern around the vehicle surface were measured for low and mean turbulence conditions, while high turbulence was used only for evaluating the vehicle admittance function.

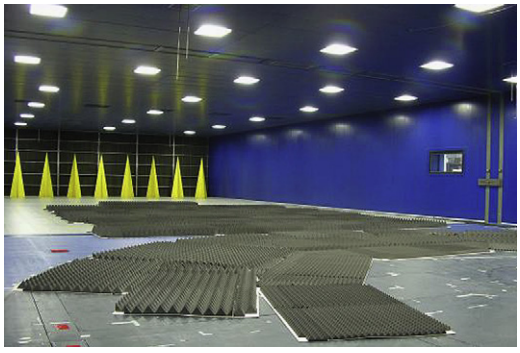

**Fig. 6.** Wind tunnel experimental set-up: boundary layer simulation.

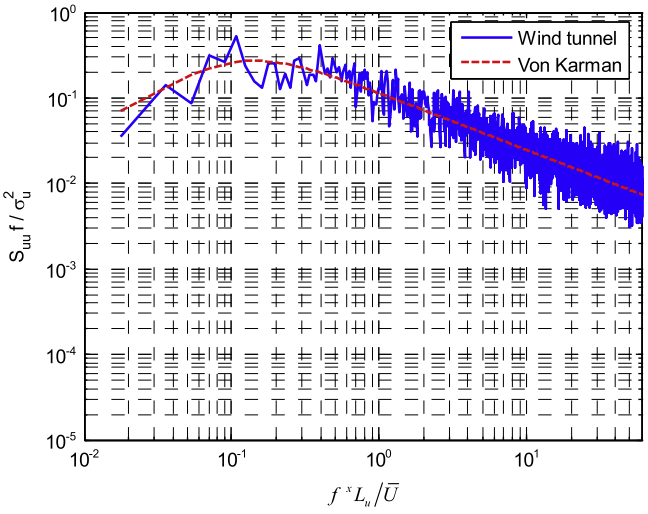


**Fig. 7.** Wind tunnel experimental set-up: normalised PSD of the streamwise longitudinal speed $S_{uu}$ at 0.25 m above the ground (model scale).

Fig. 7 shows the comparison between the normalised streamwise longitudinal velocity Power Spectral Density ($S_{uu}$, ESDU 86010), measured in mean turbulence conditions, and the interpolation of the real wind normalised Power Spectral Density provided by Von Karman, as a function of the reduced frequency. The reduced frequency $f_r$ is defined as

$$f_r = f^{x}L_u/\overline{U} \tag{1}$$

$f$ being the dimensional frequency and $\overline{U}$ being the mean wind velocity.

The two curves in Fig. 7 are in good agreement. Therefore the frequency content of the wind simulated in the wind tunnel can be assumed equivalent to the natural wind, at low reduced frequency also.

## 3. Experimental results: mean aerodynamic coefficients

In this section, the effects of the yaw angle $\alpha$ (Fig. 8) and of the boundary layer simulation (Fig. 6) on the mean aerodynamic coefficients of the VAN vehicle will be presented. Moreover, in order to get a better comprehension of the mean aerodynamic forces and moments variation with respect to the yaw angle and turbulence condition, the pressure distribution around the vehicle will be analysed.

In reference to Fig. 8, at each yaw angle, the mean aerodynamic force and moment coefficients are defined as

$$C_{Fx} = \frac{\overline{F}_x}{1/2\rho\overline{U}^2 A_f} \quad C_{Fi} = \frac{\overline{F}_i}{1/2\rho\overline{U}^2 A_l} \quad (i=y,z)$$

$$C_{Mi} = \frac{\overline{M}_i}{1/2\rho\overline{U}^2 A_l h} \quad (i=x,y,z) \tag{2}$$

where $\overline{F}_i$ is the mean value of the ith force component while $\overline{M}_i$ is the mean value of the moment about the $i$th axis, evaluated with respect to the origin O of the reference system, set at road level, in correspondence to the vehicle c.o.g. (Fig. 8). $A_l$ represents the vehicle lateral surface ($XZ$ plane, Fig. 8), $A_f$ the front vehicle surface ($YZ$ plane, Fig. 8), $h$ is the reference height, $\rho$ is the air density and $\overline{U}$ is the mean streamwise velocity at 0.25 m above the ground (model scale). Table 2 summarises the VAN model dimensions adopted for the definition of the aerodynamic coefficients.

The results of the measured flow pattern around the vehicle, are reported in terms of mean pressure coefficients $C_{p\text{-}I}$, which are

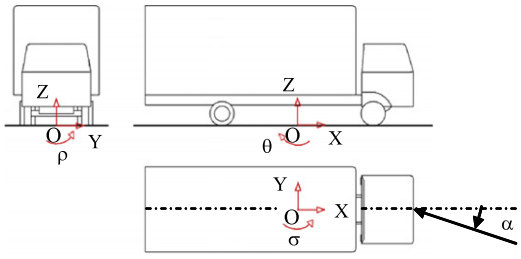


**Fig. 8.** Reference system for the aerodynamic forces and moments measurement.

**Table 2**
VAN dimensions (model scale).

| | | |
|---|---|---|
| Reference height | $h$ | 0.262 m |
| Frontal surface | $A_f$ | 0.066 m$^2$ |
| Lateral surface | $A_l$ | 0.189 m$^2$ |

defined as

$$C_{p,i} = \frac{P_i - P}{0.5\rho\overline{U}^2} \tag{3}$$

where $P_i$ is the pressure at ith tap and $P$ is the reference pressure.

### 3.1. Effect of yaw angle

The longitudinal, lateral and vertical force coefficients, as well as the roll, pitch and yaw moment coefficients for the 1:10 VAN scale model shown in Fig. 1, are reported in Fig. 9 as a function of the yaw angle. Both mean values and corresponding standard deviation error bars are indicated. Flat ground scenario and low turbulence condition are considered (reference configuration).

Fig. 9(a) shows that the longitudinal force is negative up to 70° and becomes positive for higher yaw angles: the sum of the projection of the aerodynamic force along the wind speed direction and of the component perpendicular to it generate a force pushing the vehicle. The same result was found by Coleman and Baker(1994) for an articulated lorry. Comparing Fig. 9(b) and (d), it is possible to observe that the trend of the lateral force coefficient is similar to the one of the roll moment coefficient. Thus the point of application of the lateral force remains almost constant for variable yaw angle. Fig. 9(c) shows that the vertical force coefficient is positive (directed upwards) at almost all yaw angles thus representing a lift force. Looking at Fig. 9(b)–(d), two significantly different behaviours can be observed at low and high yaw angles: up to 55°, they all grow up with an almost linear trend; when the yaw angle is increased further, the vertical force coefficient tends to drop rapidly to zero, while the lateral force and the roll moment coefficients remain almost constant. This behaviour is consistent with the one observed for rail vehicles (Bocciolone et al., 2008) and it is associated with a transition in the wind–vehicle interaction: at low yaw angles the vehicle behaves like a slender body, while at high yaw angles it acts like a bluff body.

Fig. 9(e) shows the pitch moment coefficient. At low yaw angles ($\alpha < 10°$) the vehicle pitch is dominated by the aerodynamic

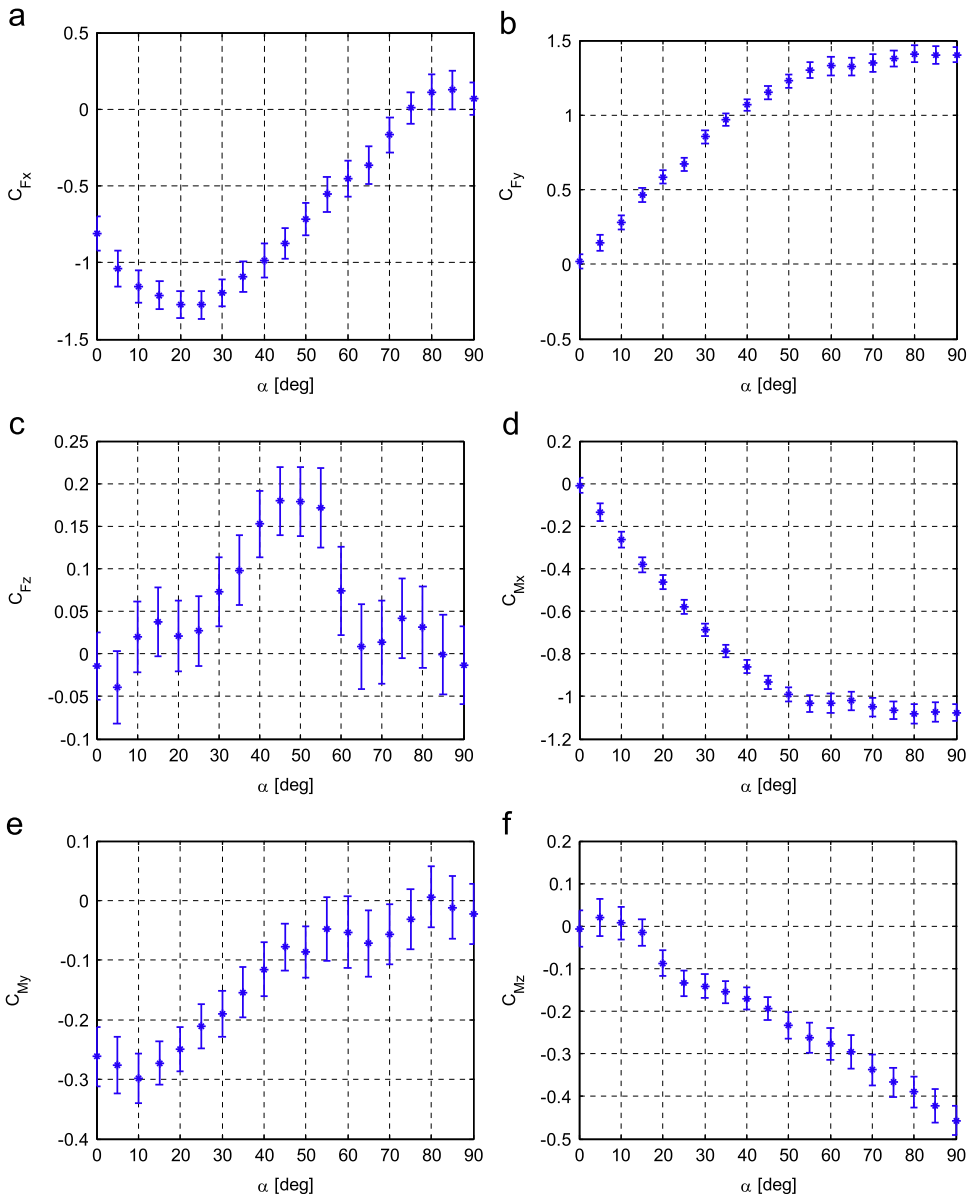


**Fig. 9.** VAN, flat ground, low turbulence: longitudinal $C_{Fx}$ (a), lateral $C_{Fy}$ (b), vertical $C_{Fz}$ (c) force coefficients and roll $C_{Mx}$ (d), pitch $C_{My}$ (e) and yaw $C_{Mz}$ (f) moment coefficients.

longitudinal force, which is negative and consequently results in a negative pitch moment coefficient. Then, in the range $\alpha = 10$–$45^\circ$, the pitch moment coefficient is also influenced by the vertical force and tends almost linearly to zero as the yaw angle increases.

As the yaw angle increases, the point of application of the lateral force moves from the vehicle cog to the vehicle back, consequently producing a negative yaw moment (Fig. 9(f)). A similar trend was found by Coleman and Baker(1994) for an articulated lorry.

The values of standard deviation are almost the same for all coefficients. While for the lateral force and the roll moment the standard deviation is small with respect to the mean value (lower than 3.5% at $\alpha = 90^\circ$ for the lateral force coefficient), for the vertical force and the pitch moment coefficients, the uncertainty is higher due to the fact that the mean value of these coefficients is small. Similar values of the standard deviations associated with the measurement uncertainty were also found in the other tested configurations.

In order to reach a deeper insight into the obtained results, the pressure distribution around the vehicle surface was also investigated. Figs. 10 and 11 respectively show the pressure coefficients around the vehicle cross section 1 (on the VAN cabin, Fig. 4) and 4 (on the VAN trailer, Fig. 4) and the longitudinal sections A and B (Fig. 4), for variable yaw angles. Positive mean pressure coefficients $C_p$ correspond to arrows directed towards the inside of the vehicle.

Looking at Fig. 10, an almost uniform distribution for all the yaw angles is observed for the leeward surface of both the VAN cabin and trailer. On the contrary, on the windward surface, pressure is negative for yaw angles lower than 20° and becomes positive for higher angles. Moreover, in correspondence with the upper windward edge, for some yaw angles, it is possible to observe a negative pressure peak. On the cabin, this peak appears for yaw angles higher than 60° (Fig. 10(a)), while on the VAN trailer it is present in the range 30–50°. This difference is due to the shape of the edges of the cabin and of the VAN trailer: smoother edges allow the flow to remain attached to the cabin until high yaw angles are reached. On the contrary, the sharp edges of the VAN trailer produce on the contrary a separation zone (with negative pressure peak) even at low yaw angles.

The pressure distributions along the longitudinal sections A and B of the VAN trailer (Fig. 11) reveal a negative pressure peak in correspondence to the front upper edge, especially in section A. Moreover, for yaw angles higher than 50–60°, the pressure over the front vertical surface of the VAN trailer becomes negative: this behaviour justifies the transition of the longitudinal force coefficient from negative to positive, which is located around 70°.

### 3.2. Effect of boundary layer simulation

A comparison between the VAN aerodynamic coefficients measured in low and mean turbulence conditions is shown in Fig. 12. Flat ground scenario is considered. The coefficients measured in mean turbulence conditions have been calculated by adopting, as the reference wind speed, the one measured by the pitot tube positioned at a height of 0.25 m (Fig. 3).

It is possible to observe that, in mean turbulence conditions, the longitudinal force (Fig. 12(a)) remains negative for the entire yaw angle range.

When considering the lateral force and the vertical force coefficients (Fig. 12(b) and (c)), the main differences arise at high yaw angles, exceeding 50°, where the vehicle behaves like a bluff body. In particular, in this range of yaw angles ($\alpha > 50^\circ$), the lateral force coefficient $C_{fy}$ measured in mean turbulence is lower than that of the corresponding coefficient measured in smooth flow: this is probably due to the differences in the wind speed vertical profiles for the two simulated turbulence conditions (Fig. 13). Since the wind speed is the same at the reference measuring point (0.25 m), the wind velocity below this height is lower in mean turbulence conditions (Fig. 13). As a consequence, the aerodynamic forces acting on the vehicle (which is the integral of pressure on the vehicle surface) are smaller in mean turbulence conditions. Moreover, with respect to low turbulence

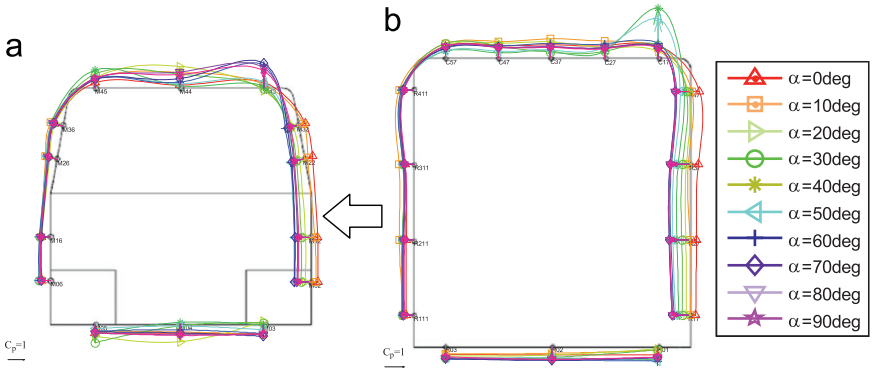


**Fig. 10.** VAN, low turbulence, flat ground: pressure coefficient $C_p$ at different yaw angles $\alpha$ for the vehicle cross section 1 (a, cabin) and 4 (b, trailer), see Fig. 4.

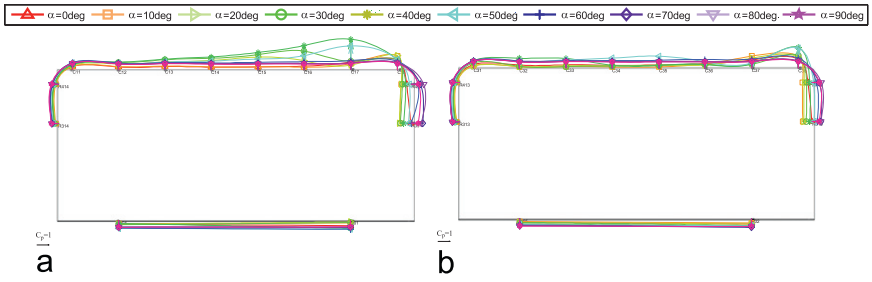


**Fig. 11.** VAN, low turbulence, flat ground: pressure coefficient $C_p$ at different yaw angles $\alpha$ for the longitudinal sections A (a) and B (b) on the VAN trailer (see Fig. 4).

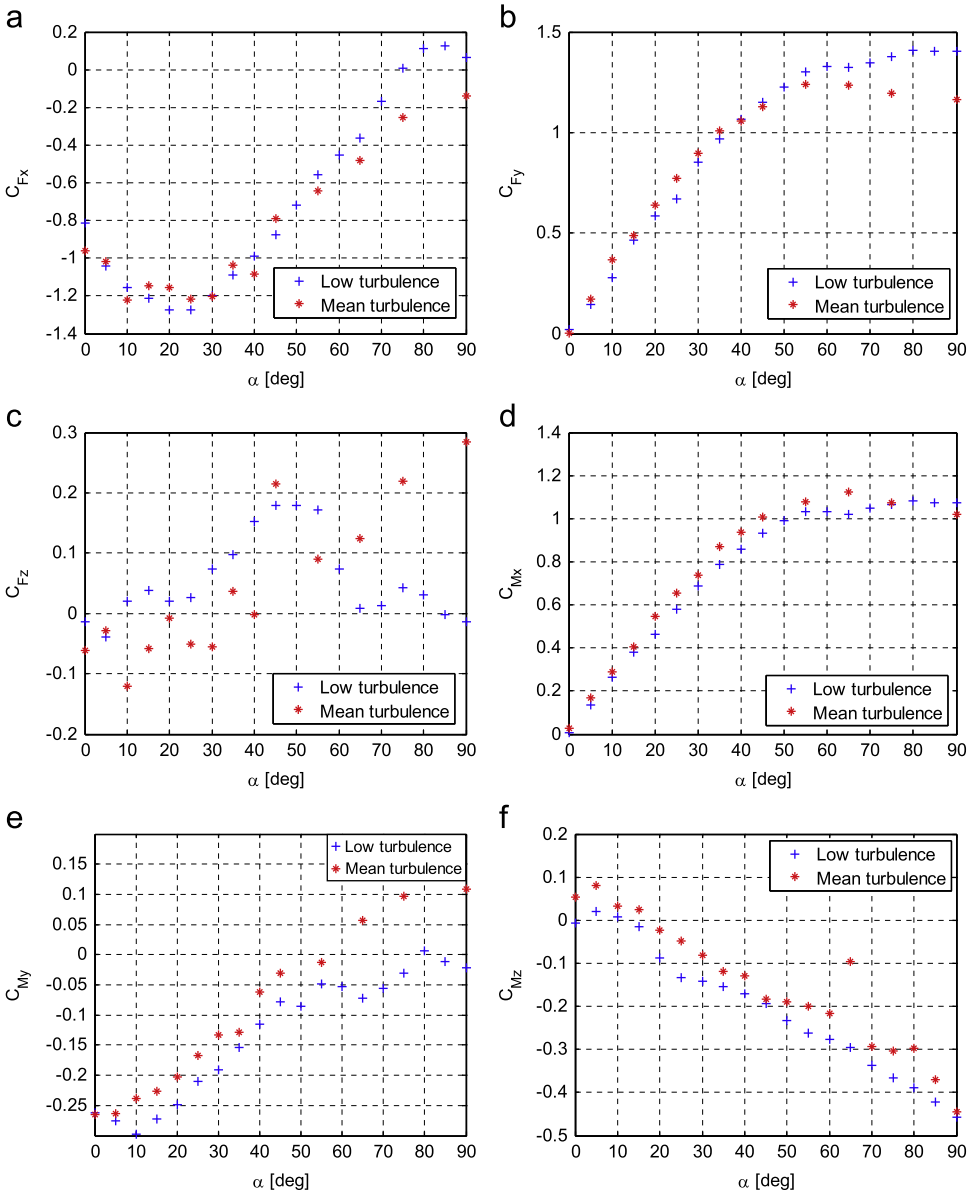


**Fig. 12.** VAN, flat ground, low turbulence vs. mean turbulence (see Table 1): longitudinal $C_{Fx}$ (a), lateral $C_{Fy}$ (b), vertical $C_{Fz}$ (c) force coefficients and roll $C_{Mx}$ (d), pitch $C_{My}$ (e) and yaw $C_{Mz}$ (f) moment coefficients.

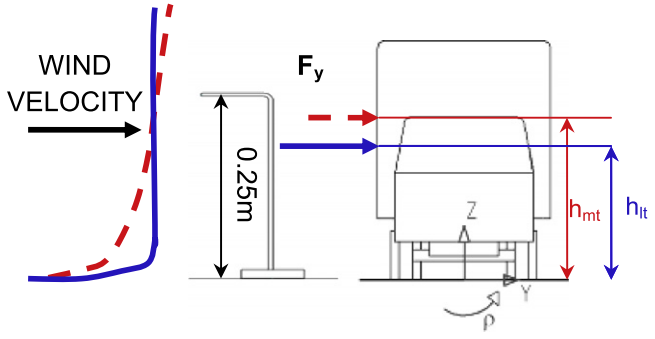


**Fig. 13.** Comparison between vertical profiles and corresponding lateral force generated in low (solid line) and mean (dashed line) turbulence conditions (see Fig. 5).

condition (Fig. 13, $h_{lt}$), the point of application of the lateral force becomes higher (Fig. 13, $h_{mt}$) due to the increasing wind speed along the vehicle height.

As far as the vertical force is concerned, it is possible to observe that, at low yaw angles, the coefficient $C_{Fz}$ measured in mean turbulence is lower in modulus and negative while, at high yaw angles, it becomes positive, with linearly increasing trend (Fig. 12(c)). At high yaw angles, the vertical force coefficient is higher in mean turbulence conditions. As it will be pointed out when looking at the pressure distributions (Fig. 14), wind turbulence affects the flow especially in correspondence to vehicle windward edge, where the flow is detaching. Higher turbulence intensity moves the detachment point, in the upper part of the vehicle, become closer to the windward edge. This results in increased negative pressure peak and the lift force.

The roll moment coefficient $C_{Mx}$ (Fig. 12(d)) is mainly associated with the lateral force acting on the vehicle. As discussed above, for high yaw angles, the lateral force is smaller in mean turbulence conditions, but its point of application is higher (Fig. 13). These two effects balance each other and, as a consequence, the roll moment coefficient is only slightly affected by turbulence condition.

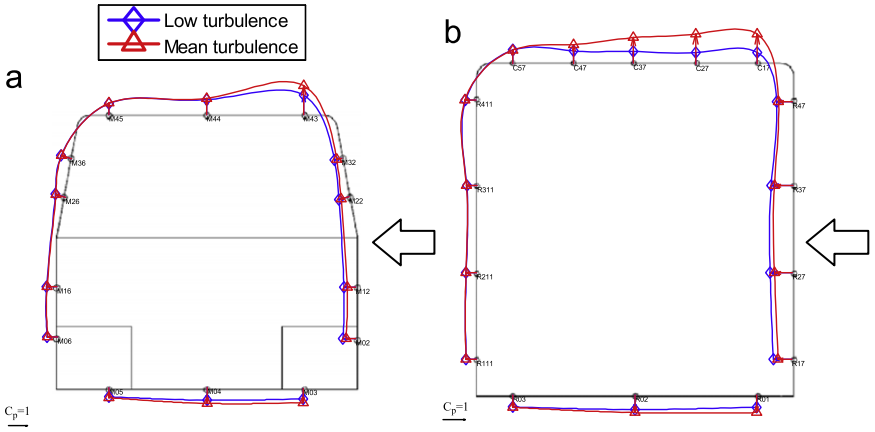


**Fig. 14.** VAN, yaw angle $\alpha$=90°, flat ground, low turbulence vs. mean turbulence: pressure coefficient $C_p$ for section 1 (a) and section 4 (b) (see Fig. 4).

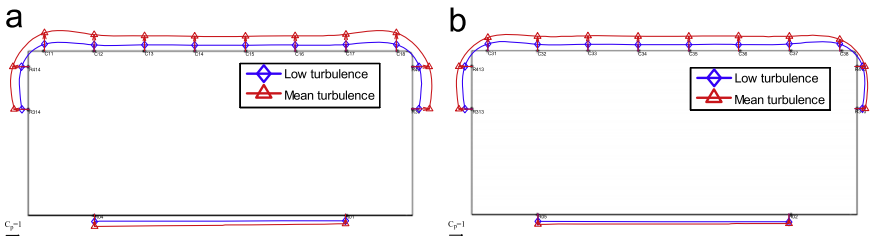


**Fig. 15.** VAN, yaw angle $\alpha$=90°, flat ground, low turbulence vs. mean turbulence: pressure coefficient $C_p$ for section A (a) and section B (b) (see Fig. 4).

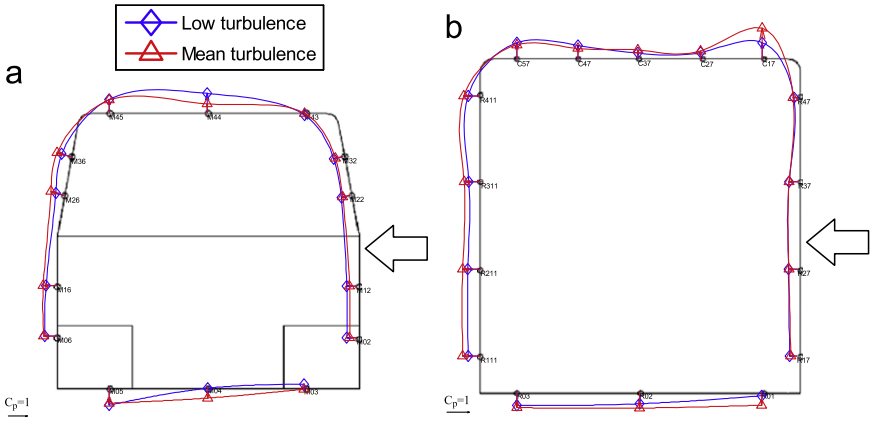


**Fig. 16.** VAN, yaw angle $\alpha$=30°, flat ground, low turbulence vs. mean turbulence: pressure coefficient $C_p$ for section 1 (a) and section 4 (b), see Fig. 4.

Finally, changes in the pitch (Fig. 12(e)) and in the yaw moment (Fig. 12(f)) coefficients due to a different turbulence are, respectively, associated to those in the vertical force and the lateral force to which they are related.

In order to support the analysis performed on boundary layer influence, the flow pattern around the vehicle was investigated. Figs. 14 and 15 show the pressure coefficients measured in sections 1 and 4 (see Fig. 4), and the ones measured along the longitudinal sections A and B (see Fig. 4). An yaw angle of 90° is considered. Diamond line refers to low turbulence while triangle line refers to mean turbulence.

Making reference to the distribution along cross sections 1 and 4 (Fig. 14), a higher pressure can be noticed on the VAN windward surface (both cabin and trailer) in low turbulence conditions, due to the wind vertical profile. On contrary, on the leeward surface, pressure is almost the same. The lateral force is higher in low turbulence than in mean turbulence conditions. In Coleman and Baker(1994), it is shown that the effect of turbulence level on the pressure distribution is higher on the leeward side than on the windward side and that the lateral force at 90° is higher in turbulent wind conditions: when comparing the results of the two experimental campaigns, it must be pointed out that the variations in the lateral force are mainly associated with the vertical profiles of wind speed, that might be different in the two campaigns.

Although the number of pressure taps is limited, from Fig. 14(b) it can be inferred that the detachment point of the flow from the windward surface is closer to the upper edge in case of the mean turbulence conditions. Moreover, both on the cabin and on the VAN trailer roof, suction is higher in mean turbulence conditions. Considering that the pressure underneath the vehicle is instead almost the same for low and mean turbulence (Figs. 14

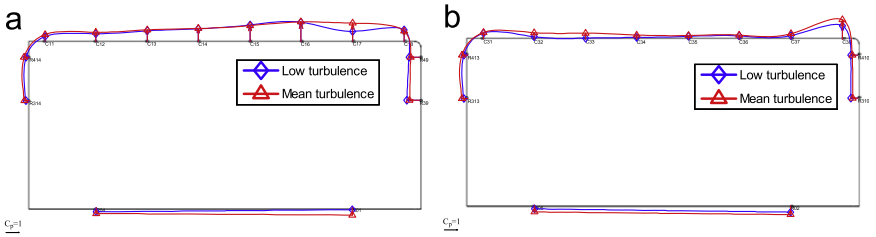


**Fig. 17.** VAN, yaw angle $\alpha=30^\circ$, flat ground, low turbulence vs. mean turbulence: pressure coefficient $C_p$ for section A (a) and section B (b) (see Fig. 4).

and 15), the lift force is higher in mean turbulence conditions. This confirms the result obtained in terms of mean aerodynamic coefficients (Fig. 12(c)). Coleman and Baker(1994), found similar data both for the vertical force and for the pressure on the roof and justified this result to be due to turbulence effects on the separated shear layer.

An opposite behaviour can be noticed for an yaw angle of 30°, when the vehicle behaves as a slender body. Pressure distributions around cross Sections 1 and 4 (Fig. 16) and longitudinal sections A and B (Fig. 17) allows in understanding the reason for this behaviour. At this yaw angle, pressure distribution on the windward surface (Fig. 16) is only slightly affected by the turbulence level, while a higher suction can be observed on the leeward surface in mean turbulence conditions. As a consequence, the lateral force is higher in mean turbulence conditions, confirming the result of Fig. 12(b).

The pressure distribution over the roof and underneath the VAN presents the main differences around the cabin (Fig. 16(a)). While in low turbulence conditions the vertical force is clearly directed upwards, in mean turbulence conditions the suction on the roof and underneath the cabin almost balance each other. On the VAN trailer, limited differences induced by the turbulence conditions can be noticed only in correspondence with the windward edge. It can thus be inferred that at 30° the variation in vertical force, as a consequence of wind turbulence intensity, is mainly associated with the pressure distribution around the cabin.

## 4. Experimental results: aerodynamic admittance function

In the ideal case of a vehicle enveloped by turbulent wind with full spatial correlation, the ith aerodynamic force/moment component can be defined according to the steady formulation, in which the mean wind speed is replaced by the instantaneous wind speed:

$$F_i=\tfrac{1}{2}\rho AC_{F_i}(\alpha)u^2(t),\quad M_i=\tfrac{1}{2}\rho AhC_{M_i}(\alpha)u^2(t),\quad i=x,y,z \tag{4}$$

where $\rho$ is the air density, $A$ is the reference area, $C_{F_i}$ and $C_{M_i}$ are the steady aerodynamic coefficients, as a function of the yaw angle $\alpha$ and $u(t)$ is the wind speed. In the more general case of turbulent wind, with a wind speed distribution which depends on space and time, the unsteady aerodynamic force can be evaluated in the frequency domain, through the corrected quasi-steady theory (Cheli et al., 2006). This approach consists of applying the steady theory and by correcting it with the admittance function (Baker, 1991b;2010; Cooper, 1984;Sterling et al., 2009; Cheli et al., 2011), this allowing to account for the spatial correlation of wind pressures at any two points on the vehicle surface. In other words, it represents a modifying adjustment of the ideal case of a vehicle enveloped by turbulent wind with full spatial correlation (Simiu and Scanlan, 1986).

The aerodynamic admittance function is defined, in the frequency domain, as the ratio between the PSD of the generic aerodynamic force/moment acting on a vehicle in conditions of turbulent wind $S_{FF}(f)$ and the corresponding PSD of the aerodynamic force evaluated through the steady theory $S_{FF\ steady}(f)$ (Cheli et al., 2006):

$$H^2(f)=\frac{S_{FF}(f)}{S_{FF\_steady}(f)}=\frac{4S_{FF}(f)}{\rho^2A^2C^2S_{u^2u^2}(f)} \tag{5}$$

where $S_{u^2u^2}(f)$ is the PSD of the square of the absolute wind speed $u$.

The admittance function is then adopted to calculate the unsteady components of the aerodynamic force through the following relation (Cheli et al., 2006):

$$F_i=\tfrac{1}{2}\rho AC_{Fi}(\alpha)u_c^2(t),\quad M_i=\tfrac{1}{2}\rho AhC_{Mi}(\alpha)u_c^2(t)\quad (i=x,y,z) \tag{6}$$

The corrected wind speed $u_c$ is defined in the frequency domain by the following equation (Cheli et al., 2006):

$$\left|U_c^2(f)\right|^2=H^2(f)\left|U^2(f)\right|^2 \tag{7}$$

where $U(f)$ and $U_c(f)$ are the Fourier transforms of $u(t)$ and $u_c(t)$. According to this equation, the admittance function can be experimentally evaluated through wind tunnel tests, by measuring both the wind speed $u(t)$ and the aerodynamic force/moment.

Tests were performed in high turbulence conditions (see Table 1), considering the flat ground scenario. Wind speed was measured through a multi-holes pressure probe, set at a height of $h=0.25$ m. 10 min time-histories were stored to allow the evaluation of the PSD.

Fig. 18 shows the admittance function evaluated experimentally for the lateral force and for the roll moment, as a function of the non-dimensional frequency $f_r$, in case of 90° of yaw angle. The values of the rations $\tilde{L}=L/^xL_u$ and $\tilde{H}=H/^xL_u$ are, respectively, 0.47 and 0.2 (see Tables 1 and 2).

The admittance function tends to 1 for low non-dimensional frequencies, i.e. for long wavelengths. In case of high non-dimensional frequencies (short wavelengths) the correlation between the wind speed measured in two generic points of the vehicle surface decreases, as well as the admittance function amplitude.

When comparing the roll moment and the lateral force admittance functions, a very similar trend can be found (Fig. 18(a)). As already noticed for steady conditions ($f_r=0$ Hz), the roll moment is in fact proportional to the lateral force. The same dependency can be observed also for unsteady conditions. As a consequence, the unsteady values of both $F_y$ and $M_x$ can be obtained (Cheli et al., 2006) through the same admittance function.

The admittance function referred to the vertical force instead presents a very different behaviour (Fig. 18(b)). At $f_r=0$, it is equal to 1 and then it increases reaching the maximum value at about $f_r=1$. A similar behaviour on the vertical component has been observed also by other authors (Coleman and Baker, 1994; Sterling et al., 2009) on different road and rail vehicles.

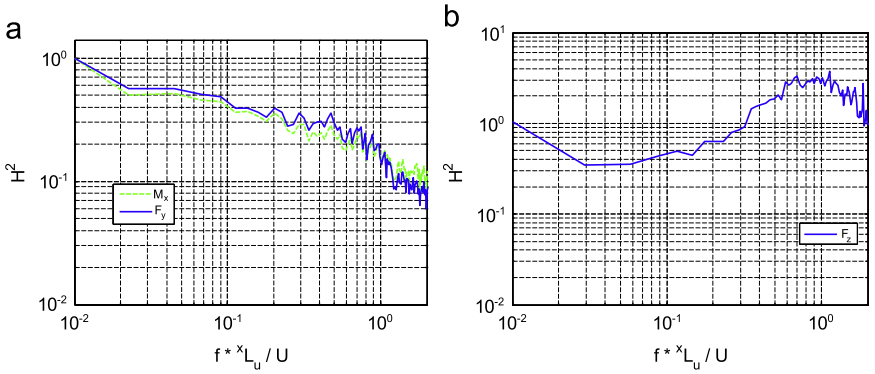


**Fig. 18.** Flat ground, VAN, high turbulence conditions, $\tilde{L} = L/{}^xL_u = 0.47$, $\tilde{H} = H/{}^xL_u = 0.2$, $\alpha = 90^\circ$: (a) admittance function of the lateral force (solid line) and the roll moment (dashed line) and (b) admittance function of the vertical force.

## 5. Conclusions

The sensitivity of steady and unsteady aerodynamic forces acting on heavy road vehicles to different test conditions is investigated in this paper and in its companion (Part II), by means of wind tunnel experiments on 1:10 scale models.

In this first part, the effects of both yaw angle and boundary layer simulation are analysed in terms of force and pressure coefficients for a high-sided lorry (VAN) set in a flat ground scenario. When increasing the yaw angle, the pressure distribution around the vehicle varies especially at the windward side (with the consequent modification of the lateral force coefficient) and in correspondence with the windward upper edge, showing the presence of a negative pressure peak for yaw angles higher than 60° on the VAN cabin and in the range 30–50° on the VAN trailer.

The effect of different turbulence conditions (low and mean) is particularly evident at high yaw angles. The lateral force and the roll moment are mainly governed by the simulated vertical wind speed profile. On the contrary, the vertical component is mainly affected by the detachment point of the flow in correspondence with the windward roof edge: this point, in mean turbulence condition, is moved upstream with a consequent increase of suction over the vehicle roof, finally leading to a higher upward directed vertical force.

The vehicle aerodynamic admittance function, useful to evaluate the unsteady components of the aerodynamic force, was measured for the main components: the lateral force and the roll moment admittance functions show a very similar trend, decreasing from 1 to 0, when the non-dimensional frequency is increased from 0 to infinity. On the contrary, the admittance function relevant to the vertical force starts from 1 at 0 non-dimensional frequency and then presents a maximum in correspondence with unit non-dimensional frequency. The vertical force does not depend on the pressure acting on the lateral surface, but is mainly influenced by the pressure distribution underneath and on top of the vehicle.

In the second part of this work (Part II), the effect of the infrastructure scenario (flat ground, embankment, single and double viaduct) and of the position (vehicle placed upwind or downwind) will be investigated, considering the same high-sided lorry described in this paper. Moreover, steady and unsteady aerodynamic forces acting on different heavy vehicles (tank truck, tractor–trailer combination and tractor–semitrailer combination) will be compared with the ones of the considered VAN to assess the effect of geometry.

## Acknowledgements

The work described in this paper was founded within the EC project WEATHER (Delaunay et al., 2006) and the Italian National PRIN Project "Improvement of safety, comfort and handling of the heavy vehicles".

## References

Baker, C.J., 1991a. Ground vehicles in high cross winds, Part 1: steady aerodynamic forces. Journal of Fluids and Structures 5, 69–90.

Baker, C.J., 1991b. Ground vehicles in high cross winds, Part 2:unsteady aerodynamic forces. Journal of Fluids and Structures 5, 91–111.

Baker, C.J., Reynolds, S., 1992. Wind induced accidents of road vehicles. Accident Analysis and Prevention 246, 559–575.

Baker, C.J., 1994. The quantification of accident risk for road vehicles in cross wind. Journal of Wind Engineering and Industrial Aerodynamics 52, 93–107.

Baker, C.J., 2002. The wind tunnel determination of crosswind forces and moments on a high speed train. Notes on Numerical Fluid Mechanics, 79. Springer-Verlag, Berlin, pp. 46–60.

Bocciolone, M., Cheli, F., Corradi, R., Muggiasca, S., Tomasini, G., 2008. Crosswind action on rail vehicles: wind tunnel experimental analyses. Journal of Wind Engineering and Industrial Aerodynamics 96, 584–610.

Cheli, F., Belforte, P., Melzi, S., Sabbioni, E., Tomasini, G., 2006. A numerical–experimental approach for evaluating cross wind aerodynamic effects on heavy vehicles. Journal of Vehicle System Dynamics Suppl., 44, 791–804.

Cheli, F., Corradi, R., Tomasini, G., 2011. Numerical model of the admittance function for the evaluation of the aerodynamic loads on vehicles due to cross wind.in: Proceedings of the 13th International Conference on Wind Engineering (ICWE13), Amsterdam, Holland, July 10–15, 2011.

Coleman, S.A., Baker, C.J., 1992. The reduction of accident risk for high sided road vehicles in cross winds. Journal of Wind Engineering and Industrial Aerodynamics 41–44, 2685–2695.

Coleman, S.A., Baker, C.J., 1994. An experimental study of the aerodynamic behaviour of high sided lorries in cross winds. Journal of Wind Engineering and Industrial Aerodynamics 53, 401–429.

Cooper, R., 1984. Atmospheric turbulence with respect to moving ground vehicles. Journal of Wind Engineering and Industrial Aerodynamics 17, 215–238.

Delaunay, D., Baker, C.J., Cheli, F., Morvan, H., Berger, L., Casazza, M., Gomez, C., Cleac'h C.Le, Saffell, R., Grégoire, R., Vinuales, A., 2006. Development of wind alarm systems for road and rail vehicles: presentation of the WEATHER project. In: Proceedings of the SIRWEC 2006, 13th International Riad Weather Conference, Torino, Italy.

DEUFRAKO Consortium, 2004. Common DEUFRAKO research on cross wind effects on high speed railway operation 2001–2004. In: Thorsten Tielkes, Pierre-Etienne Gautier (Eds.), Final Report of DEUFRAKO SIDE WIND project, Draft version V 1.0.

ESDU 86010. Characteristics of atmospheric turbulence near the ground. Part 3: variations in space and time for strong winds (neutral atmosphere) Engineering Sciences Data Unit, London.

Gautier, P.-E., Tielkes, T., Sourget, F., Allain, E., Grab, M., Heine, C., 2003. Strong wind risks in railways: The DEUFRAKO crosswind program. In: Proceedings of the sixth World Congress on Railway Research, Edinburgh, pp. 476–485.

Quinn, A.D., Sterling, M., Robertson, A.P., Baker, C.J., 2007. An investigation of the wind induced rolling moment on a commercial vehicle in the atmospheric boundary layer. Proceedings of the Institution of Mechanical Engineers, Part D, Journal of Automobile Engineering 221 (11), 1367–1379.

RAPIDE Consortium, 2001. Synthesis Report from the Aerodynamics Workshop, Koln.

Simiu, E., Scanlan, R., 1986. Wind Effects on Structures. Wiley-Interscience Publication, New York.

Sterling, M., Baker, C.J., Bouferrouk, A., ONeil, H., Wood, S., Crosbie, E., 2009. An investigation of the aerodynamic admittances and aerodynamic weighting functions of trains. Journal of Wind Engineering and Industrial Aerodynamics 97, 512–522.

Sterling, M., Quinn, A.D., Baker, C.J., Hargreves, D.M., Cheli, F., Sabbioni, E., Tomasini, G., Delaunay, D., Morvan, H., 2010. A comparison of different methods to evaluate the wind induced forces on a high sided lorry. Journal of Wind Engineering and Industrial Aerodynamics 98 (1), 10–20.

Tielkes T. and Gautier P.-E., 2005. Common DeuFraKo Research on Cross Wind Effects on High Speed Railway Operation 2001–2004. Report issued by Deutsche Bahn AG, DB Systemtechnik and SNCF, Direction de l'Innovation et de la Recherche, Munich, Paris.

TRANSAERO Consortium, 2002. TRANSAERO a European initiative on transient aerodynamics for railway system optimization. In: Schulte Werning, B., Gregoire, R. (Eds.), Notes on Numerical Fluid Mechanics, vol. 79. Springer, Berlin, pp. 27–38.